D-shaped fiber optic SPR biosensors based on a metal-graphene structure

Dejun Feng (冯德军)[1*], Guanxiu Liu (刘冠秀)[1], Maosen Zhang (张茂森)[1], and Dongfang Jia (贾东方)[2]

[1]*School of Information Science and Engineering, Shandong University, Jinan 250100, China*

[2]*College of Precision Instrument and Optoelectronics Engineering, Tianjin University, Tianjin 300072, China*

[*]*Corresponding author: dejunfeng@sdu.edu.cn*

Received July 18, 2013; accepted October 17, 2013; posted online November 8, 2013

We design a D-shaped fiber optic biosensor based on the surface plasmon resonance (SPR) of a metal-graphene layer and simulate this SPR using the finite element method. Using a metal-graphene layer as the sensing material, surface plasma resonance is simulated as the refractive index of the external environment ranges from 1.33 to 1.36. Simulation results show that a metal-graphene layer attached to the D-shaped optical fiber core can couple with light under a specific polarization state and excite strong plasma oscillations on the layer surface. Calculated transmission coefficients show that the resonance wavelength obviously moves toward longer wavelengths as the refractive index of the test medium increases, and a sensitivity of 5400 nm/RIU is obtained. Because of its large surface volume ratio and good biocompatibility, graphene may be utilized in many applications in the field of biosensing.

OCIS codes: 060.0060, 060.2370, 170.0170.

doi: 10.3788/COL201311.110607.

Rapid developments in modern electronics and biotechnology have allowed the emergence of fiber optic biosensor technology as an independent high-tech field[1]. Fiber optic biosensors can be divided into evanescent wave[2], fluorescence labeled[3], and surface plasmon resonance[4] (SPR) sensors according to the operating principle. SPR technology is widely used in optical biosensors because it features advantages such as absence of marking, high sensitivity, high specificity, and real-time results[5].

Graphene film is a monolayer of carbon atoms packed into a dense honeycomb crystal structure that can be viewed as an individual atomic plane extracted from graphite. As a novel material with unique optical and electrical properties, graphene has been extensively studied in a number of areas[6,7]. It possesses advantages of large surface volume ratio and good biocompatibility and thus allows fixing of large amounts of biomolecules. Biosensors based on graphene are known to have wide linear ranges and low detection thresholds. Thus, graphene provides a good platform from which to build a variety of biosensors[8].

Each carbon atom of graphene features an unfilled electron structure. As such, graphene is a typical zero-band gap semi-metallic material that can replace traditional precious metals to produce SPR[9]. Pradeep Kumar Maharana *et al.* developed a chalcogenide prism and graphene multilayer-based SPR biosensor in 2012[10]. Graphene increases the absorption of biomolecules, thereby improving the sensitivity of the resulting biosensor. Jang Ah Kim *et al.* reported an SPR based fiber optic sensor coated with graphene[11]. When streptavidin-biotin and double-cross DNA are combined, the refractive index increases and the resonance wavelength at 7.726 nm moves toward longer wavelengths.

While combining graphene biosensor technology with optical fibers shows good prospects for sensing applications[12], domestic research on graphene-based optical biosensors is fairly limited. Traditional optical fiber sensors have advantages of large transmission capacity, rapid measurement, anti-electromagnetic interference, and miniaturization. Thus, this letter designs a fiber optic biosensor based on the SPR effect on a metal-graphene layer. The resulting sensor is expected to be widely used in the chemical, biomedical, environmental safety, and food safety industries as well as in many other aspects.

Surface plasmon polaritons (SPPs) are electromagnetic waves excited by the interaction between light and free electrons on a metal surface typically presenting in the interface of a metal and dielectric layer[13]. Given their high sensitivity depending on the surface environment, SPPs are widely used in biosensors.

Figure 1 shows the interface of the metal-dielectric. The incident light is decomposed into s-polarized light (TE wave) whose electric vector E is perpendicular to the incident plane, and p-polarized light (TM wave) whose E is in the incident plane. Since the s-polarized E is parallel to the direction of the interface, it does not hinder the movement of electrons and cannot excite surface plasmon waves (SPWs); thus, SPR phenomena cannot occur. In p-polarized light, the E has a component in the vertical direction of the interface, and electrons around the nucleus vibrate perpendicular to the interface driven by the electric field of light. On the metal surface, the transverse movement (perpendicular to the interface) of electrons is blocked by the surface to form a gradient distribution of the electron concentration. This distribution causes plasma oscillation or SPWs on the metal surface.

SPPs are non-radiative electromagnetic waves constrained to the surface of a conductor. Generally, surface plasmons are accompanied by a longitudinal (TM or p-polarized) electric field, which decays exponentially in metal as well as in dielectrics. Because of the exponential decay of the field intensity, the field has its maximum at metal-dielectric interface itself. High losses in the metal cause SPWs to propagate with high attenuation in the visible and near-infrared spectral regions, eventually depleting SPWs within a limited range of propagation

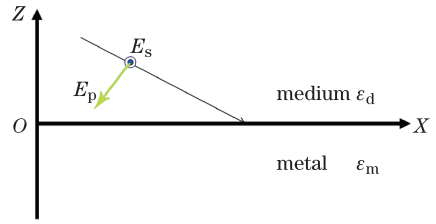

Fig. 1. Interface of metal-dielectric.

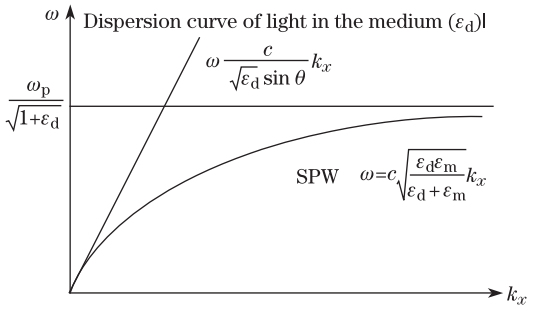

Fig. 2. Dispersion curves of SPW and direct light incident through the dielectric medium.

distances, usually in the micrometer or nanometer scale[14].

By solving Maxwell's equation, the propagation constant of the surface plasma wave propagating at the interface between the dielectric and metal is given by the following expression:

$$k_{spp} = k_0 \left(\frac{\varepsilon_d \varepsilon_m}{\varepsilon_d + \varepsilon_m}\right)^{1/2}, \quad (1)$$

where k_0 denotes the free space wave number, ε_m is the dielectric function of the metal, and ε_d is the dielectric constant of the medium. ε_m can be expressed as

$$\varepsilon_m = 1 - \frac{\omega_p^2}{\omega^2 - i\gamma\omega}, \quad (2)$$

where ω_p is the plasma frequency, γ is the collision frequency of electrons or damping factor, and ω is the angular frequency of incident light. The dispersion curve of SPW is shown in Fig. 2.

According to Fig. 2, for a given frequency, the propagation constant of surface plasmons is greater than that of the light wave directly incident on the dielectric medium. Hence, direct light cannot excite surface plasmonson a metal-dielectric interface. Thus, to excite surface plasmons, the wave vector of the exciting light in a dielectric medium must be increased. Coupling devices, such as prisms (Otto and Kretschmann type), waveguides (optical fiber), and gratings, maybe used to excite SPPs[15].

This letter designs a D-type fiber to excite SPPs, and the relevant structure is shown in Fig. 3. The potential fabrication process of the sensing head is as follows: The D-shaped optic fiber can be obtained by side-polishing technology. The surface of the D-shaped optical fiber is coated with a layer of metal, such as An or Ag, by magnetron sputtering at room temperature. The graphene film fabricated by chemical vapor deposition (CVD) is transferred onto the metal surface using the wet chemical method[16] to finally achieve the metal-graphene structure.

When light propagates through a fiber, most of the light forms a total internal reflection (TIR), and part of the light takes the form of evanescent waves through the cladding layer. The x-component of the wave propagation constant of the evanescent wave between the core and metal-graphene layer is expressed as

$$k_x = \frac{\omega}{c}\sqrt{\varepsilon_1}\sin\theta, \quad (3)$$

where ε_1 is the dielectric constant of the fiber core.

From $k_{spp} = k_x$, we can conclude that the conditions necessary to achieve the SPR phenomenon are

$$\frac{\omega}{c}\sqrt{\varepsilon_1}\sin\theta = \frac{\omega}{c}\sqrt{\frac{\varepsilon_{gm}\varepsilon_4}{\varepsilon_{gm}+\varepsilon_4}}, \quad (4)$$

then

$$\sin\theta_{spr} = \sqrt{\frac{\varepsilon_{gm}\varepsilon_4}{\varepsilon_{gm}+\varepsilon_4}}\Big/ n_1, \quad (5)$$

where θ_{spr} is the resonance angle and ε_{gm} is the dielectric constant of the metal-graphene layer.

A broadband light source (in case the wavelength modulation method is used) is launched into one end of the optical fiber. TIR takes place and light propagates with a critical angle (depending upon the numerical aperture of the fiber). Light with different wavelengths presents different wave vectors. When the wave vector of light matches the wave vector of the SPWs, light is attenuated rapidly and forms an SPR valley. Differences in refractive index yield differences in the resonance wavelengths. Since biological macromolecule interactions on the surface of fiber optic SPR sensors can cause large changes in the refractive index, biological reactions may be analyzed quantitatively according to changes in the resonance wavelength.

We use the finite element method (FEM) to simulate physical phenomena by solving the partial differential equation (single field) or partial differential equations (multi-fields). Multimode fibers are usually used in optical fiber biosensor systems, so we select a multimode fiber (core diameter, 16 μm; cladding thickness, 40 μm) as a model for simulation analysis. The sensor geometry and mesh division are shown in Fig. 4.

The core refractive index n_1 is 1.4457, and the refractive index of the cladding n_2 is 1.4378, scattering boundary conditions around the fiber, and the incident wavelength of light ranges from 600 nm to 1 μm. The right

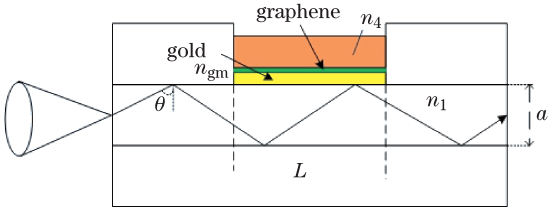

Fig. 3. Structure of the D-type optical fiber sensor.

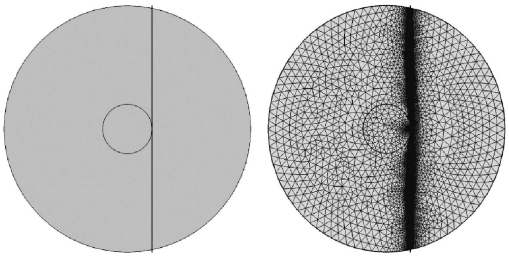

Fig. 4. D-type optical fiber sensor geometry and mesh division.

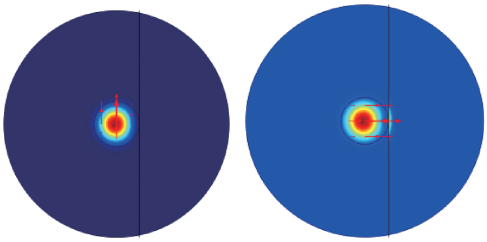

Fig. 5. Base mode of the D-shaped fiber distribution.

side of the core in Fig. 4 is a gold film attached to monolayer graphene with a thickness of 0.34 nm and a refractive index $n = 3 + C_1\lambda/3$, where C_1 is 5.446 μm^{-1} and λ is the incident wavelength[17]. The semicircle at the right side of the metal-graphene film refers to the test medium, which changes the refractive index n_3 from 1.33 to 1.36. In this section, we analyze the mode field based on the above mentioned model.

The fundamental mode in the optical fiber is composed of two mutually orthogonal polarization mode components, as shown in Fig. 5. The surface arrows represent the polarization direction of the electric field. The direction of electric field polarization is parallel to the metal-graphene film in the left image but perpendicular to the metal-graphene layer in the right. From conventional surface Plasmon theory, only the electric field perpendicular to the metal-dielectric interface (TM mode) can excite SPPs and result in SPR phenomenon. From the right-hand figure, significant energy is observed between the metal-graphene layer and the test medium, which indicates the excitation of surface plasmons at this position. Meanwhile, consistent with theory, the mode on the left image with the field direction parallel to the interface cannot excite surface plasmons. Figure 6 shows typical high-order modes of distribution in the D-shaped fiber. Similar to the fundamental mode, only the higher-order polarization mode in which the electric field is perpendicular to the interface can excite surface plasmons.

Figure 7(a) shows the intensity distribution of the metal-graphene SPPs excited in fundamental mode. Strong light is coupled out of the core by the metal-graphene structure. During conventional SPR simulation based on Au film operated by Santos *et al.*[18], results of which are shown in Fig. 7(b), the light coupled out was lower than that in our simulation, which shows the superiority of the metal-graphene structure for SPR sensing. Addition of a graphene layer to metal can enhance SPPs and increase the sensitivity of sensors based on SPR. The large surface volume ratio and good biocompatibility of graphene is also of greatusein building highly sensitive biosensors.

D-shaped fibers combined with a metal-graphene layer can be used to build a high-performance biosensor.

A four-layer Kretchmann configuration of the D-type SPR fiber sensor is shown in Fig. 3. Using Fresnel's equations, the reflective coefficient of p-polarization can be expressed as[19]

$$r_{1234} = \frac{r_{12} + r_{234}\mathrm{e}^{\mathrm{i}2k_2d}}{1 + r_{12}r_{234}\mathrm{e}^{\mathrm{i}2k_2d}}, \tag{6}$$

where $r_{234} = \frac{r_{23}+r_{34}\mathrm{e}^{\mathrm{i}2k_3d}}{1+r_{23}r_{34}\mathrm{e}^{\mathrm{i}2k_3d}}$ and $r_{ij} = \frac{n_i^2/k_i - n_j^2/k_j}{n_i^2/k_i + n_j^2/k_j}$. k_i is the component of the wave vector in medium i in the z direction and is given as

$$k_i = k_0\left(n_i^2 - n_1\sin^2\theta\right)^{1/2} = \frac{2\pi}{\lambda}\left(n_i^2 - n_1\sin^2\theta\right)^{1/2}, \tag{7}$$

where n_1, n_2, n_3, and n_4 represent the refractive indices of the core, the metal, graphene, and the external test medium, respectively. θ is the angle of incidence on the interface in Fig. 3.

Light passing through a fiber coated with a metallic film shows a decay in intensity; this phenomenon is called the attenuated total reflection (ATR) effect. In once time of ATR, the reflectivity of p-polarization is written as $R_\mathrm{p} = |r_{1234}|^2$. If the sensor is L long, the number of ATR as function of θ and a(the core diameter) is written as $m = L/2a\tan\theta$. Then, the total reflectivity of p-polarization is written as $R = R_\mathrm{p}^m$.

In this simulation, L=5 mm, a=16 μm, and θ=60°. When the refractive index of the external environment changes, the transmission coefficients at different wavelengths also change accordingly.

As shown in Fig. 8, when the refractive index of test medium increases from 1.33 to 1.36, the resonant wavelength obviously moves from 675 to 837 nm, and a sensitivity of 5400 nm/RIU may be obtained.

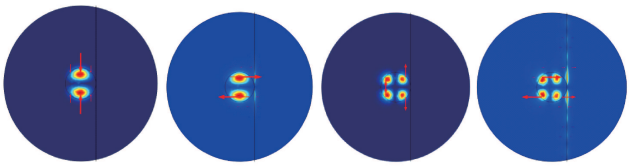

Fig. 6. Typical high-order mode distributions in the D-shaped fiber.

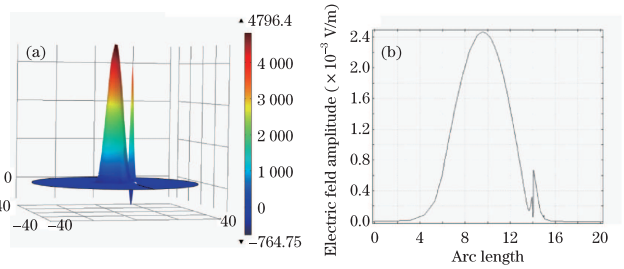

Fig. 7. Intensity of (a) metal-graphene SPPs and (b) Au excitation in fundamental mode.

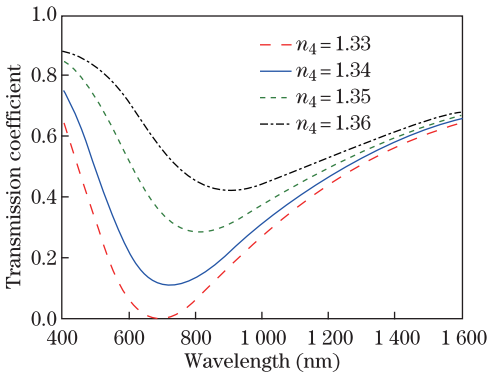

Fig. 8. Transmission coefficients of the sensor under different refractive indices in the test medium.

In conclusion, this letter describes the potential applications of graphene in the field of biosensing. We designed a novel D-shaped fiber optic SPR biosensor using a metal-graphene structure and simulated SPR phenomena on the metal-graphene layer using the finite element method. Simulation results show that a metal-graphene layer attached to a D-shaped optical fiber core can couple with the light under a specific polarization state and excite strong plasma oscillations on the layer surface. Transmission coefficient calculations show that when the refractive index of the test medium increases, the resonance wavelength obviously moves toward longer wavelengths. Considering its large surface to volume ratio and good biocompatibility, graphene may be expected to have important applications in the field of biosensing.

This work was supported by the Natural Science Foundation of Shandong Province, China (No. ZR2011FM013) and the Innovation Foundation of China Electronics Technology Group Corporation No. 46 Research Institute (No. CJ20130303).

References

1. Otto S. Wolfbeis, Analytical Chemistry **80,** 4269 (2008).
2. Yu-Zheng Su, Min-Wei Hung, and Kuo-Cheng Huang, Phys. Proc. **19,** s379 (2001).
3. SunghoKo and Sheila A. Grant, Biosens. and Bioelectron. **21,** 1283 (2006).
4. Y. Chen, R. Zheng, Y. Lu, P. Wang, and H. Ming, Chin. Opt. Lett. **9,** 100605 (2011).
5. Alexandre G. Brolo, Nature Photon. **6,** 709 (2012).
6. Bonaccorso F., Sun Z., Hasan T., and Ferrari A. C., Nature Photon. **4,** 611 (2012).
7. Y. K. Yap, Richard M. De La Rue, C. H. Pua, S. W. Harun, and H. Ahmad, Chin. Opt. Lett. **10,** 041405 (2012)
8. Chun-Hua Lu, Huang-HaoYang, Chun-Ling Zhu, Xi Chen, and Guo-Nan Chen. Angewandte Chemie International Edition **48,** 4785 (2009).
9. A. N. Grigorenkol, M. Polini, and K. S. Novoselov, Nature Photon. **6,** 749 (2012).
10. Pradeep Kumar Maharana and RajanJha, Sensors and Actuators B **169,** 161 (2012).
11. Jang Ah Kim, Taehyun Hwang, Sreekantha Reddy Dugasani, Rashid Amin, Atul Kulkarni, Sung Ha Park, and Taesung Kim, Sensors and Actuators B **187,** 426 (2013).
12. C. S. Yan1 and J. M. Gong, Mater. Technol. **26,** 173 (2011).
13. Mark L. Brongersma and Vladimir M. Shalaev, Science **328,** 440 (2010).
14. Anatoly V. Zayatsa, Igor I. Smolyaninovb, and Alexei A. Maradudinc, Physics Reports **408,** 131 (2005).
15. William L. Barnesl, Alain Dereux, and Thomas W. Ebbesen, Nature **424,** 824 (2003).
16. Feng De-Jun, Hang Wen-Yu, Jiang Shou-Zhen, Ji Wei, and Jia Dong-Fang, Acta Phys. **62,** 054202 (2013).
17. M. Bruna and S. Borini, Appl. Phys. Lett. **94,** 031901 (2009).
18. D. F. Santos, A. Guerreiro, and J. M. Baptista, Photon. Sens. **3,** 61 (2013).
19. Ming-Hung Chiu, Chih-Hsien Shih, and Ming-Hsin Chi, Sensors and Actuators B **123,** 1120 (2007).